

Mean Stress and the Exhaustion of Fatigue-Damage Resistance

Avraham Berkovits
Lewis Research Center
Cleveland, Ohio

November 1989

(NASA-TM-101311) MEAN STRESS AND THE
EXHAUSTION OF FATIGUE-DAMAGE RESISTANCE
(NASA) 18 p

CSCL 20K

N90-13819

Unclas
0252602

G3/39





MEAN STRESS AND THE EXHAUSTION OF FATIGUE-DAMAGE RESISTANCE

Avraham Berkovits*
National Aeronautics and Space Administration
Lewis Research Center
Cleveland, Ohio 44135

SUMMARY

Mean-stress effects on fatigue life are critical in isothermal and thermo-mechanically loaded materials and composites. Unfortunately, existing mean-stress life-prediction methods do not incorporate physical fatigue-damage mechanisms. An objective of this paper is to examine the relation between mean-stress-induced damage (as measured by acoustic emission) and existing life-prediction methods. Acoustic emission instrumentation has indicated that, as with static yielding, fatigue damage results from dislocation buildup and motion until dislocation saturation is reached, after which void formation and coalescence predominate. Correlation of damage processes with similar mechanisms under monotonic loading led to a reinterpretation of Goodman diagrams for 40 alloys and a modification of Morrow's formulation for life prediction under mean stresses. Further testing, using acoustic emission to monitor dislocation dynamics, can generate data for developing a more general model for fatigue under mean stress.

INTRODUCTION

Significantly large mean stresses can develop under creep-fatigue loading conditions at high temperatures. This is especially so under thermal and bithermal cycling, wherein the ratio of elastic to plastic strain range can vary between the tension and compression halves of the cycle (ref. 1). Mean stresses that develop during large inelastic strain cycles tend to be ineffective in influencing cyclic life. Under low strains, however, mean stresses can influence crack-initiation fatigue lives to a greater extent than do creep effects. When the mean stresses are tensile, crack-initiation life is shortened and accurate prediction of this effect becomes of prime importance.

Different mean-stress effects have been documented for a variety of materials and testing techniques with the result that numerous mean-stress theories have emerged for nominally elastic, isothermal, high-cycle fatigue loading. Additionally, it has been suggested that, for elastic thermal cycling, mean-stress effects may be estimated by replacing the mean-stress ratio (see ref. 1) in the Morrow mean-stress relation (ref. 2) with the analogous mean elastic strain ratio. The mean elastic strain appears in the equation as a linear effect in thermal cycling, as does mean stress in the elastic isothermal case. In isothermal fatigue, the two formulations are, of course, identical.

The Morrow mean-stress formula must be further modified for thermomechanical cycling in the inelastic, low-cycle regime. Inelastic strain cycling involving plasticity and creep strain introduces strainrate-dependent flow

*National Research Council - NASA Research Associate, on leave from Technion - Israel Institute of Technology, Haifa, Israel.

strengths. Also, the ratio of inelastic strainrange to elastic strainrange has been shown to be significant in governing the amount of mean stress that can develop and be sustained (ref. 1). These parameters are closely related to the structural and metallurgical changes taking place in the microstructure during cycling.

In many engineering applications, inelastic strain cycling phenomena are minimal because fatigue lives are in the nominally elastic, high-cycle regime. Nevertheless, even in the high-cycle fatigue regime, damage is incurred by plastic deformation mechanisms, and, if the temperature is sufficiently high, by creep and oxidation. However, the inelastic strains that are developed may be too small to be discerned by conventional laboratory extensometry.

A research effort was initiated in which the effects of various fatigue parameters were isolated and evaluated. Parametric influence on the development of mean stresses and their subsequent effect on isothermal and thermo-mechanical fatigue life were determined. An attempt was made to formulate a model representing the observed responses. This report also contains a review of microscopic fatigue damage mechanisms and their relation to a macroscopic response that is measurable in the mechanical testing laboratory. Particular attention is given to the significance of acoustic emission as a measure of dislocation dynamics. An outline is proposed for using acoustic emission data obtained in strength tests for predicting crack-initiation fatigue life in the presence of mean stress in fatigue situations. The emphasis is on high-cycle fatigue, where mean-stress effects are particularly large.

Mean Stress in Classical Isothermal Fatigue

The fact that mean stresses affect fatigue life was recognized almost immediately after the fatigue problem was first recognized. Wöhler reported the first fatigue test data in 1870, and by 1874 Gerber published results which showed that tensile mean stress shortens fatigue life. John Goodman, in his book "Mechanics Applied to Engineering" (ref. 3), presented a graph (fig. 1) which showed the effect of mean stress upon the 4×10^6 -cycles-to-failure endurance limit of steel. This type of graph was later modified by others to describe the effect of mean stress at any lifetime, and became known as the modified Goodman diagram (fig. 2).

It is well known that the influence of mean stress on fatigue life is a function of the stress (or strain) amplitude relative to material yielding. Although at moderate-to-low amplitudes tensile mean stresses shorten life and compressive mean stresses lead to longer lives, their effect tends to disappear at high amplitudes in low-cycle fatigue (fig. 3 and ref. 1). In a related effect, mean stresses cannot be sustained for long under high-amplitude, strain-controlled cycling, but soon cyclically relax, tending toward a symmetrical stress cycle about zero stress (fig. 4).

Damage Mechanisms

In order to understand the nature of the mean-stress effect in fatigue, the various damage stages occurring during fatigue must be considered. Commonly, fatigue life is characterized by outward evidence of fatigue damage and is divided into two stages, crack initiation and crack propagation. On the

other hand, the various internal damage processes are related to the mechanisms that control cyclic plastic deformation (ref. 5).

Dislocation dynamics are responsible for initiating plastic deformation in the low strainrange. Many pure metals and fully soluble metal alloys exhibit a type of plastic deformation that occurs in parallel slip bands and is induced by ordered dislocation glide (refs. 6 and 7). Most engineering alloys deform plastically because of dislocation multiplication and cross slip. These plastic deformation mechanisms are only discernible at electron-microscope magnification levels (ref. 8). Regardless of whether one or both of these damage processes are operating in a given material, sufficient dislocations eventually coalesce in various locations to form a number of voids, or microscopic cracks. At this stage, there are so many dislocations in the material lattice structure that the back stress set up in the stress field around the voids inhibits further dislocation multiplication and momentum change. At this point, evidence of strain hardening is seen.

Further plastic deformation results from void migration and microcrack coalescence rather than from dislocations. After sufficient coalescence has occurred, a third stage of fatigue damage sets in, as one or more of the microcracks reaches a length that is visible to the naked or optically assisted eye and becomes a "well-behaved" crack. This point defines the crack-initiation fatigue life and is the result of three consecutive fatigue-damage mechanisms.

The final phase of fatigue damage occurs as the dominant crack grows in length under continued cyclic loading, eventually reaching the "critical crack size" at which separation occurs because the material or structure can no longer support the applied load. The number of cycles required to traverse this phase defines the macroscopic crack-propagation life. This is dealt with by fracture mechanics methods and is not discussed herein. The present work treats only the earlier fatigue-damage mechanisms that lead to crack initiation.

Fatigue Damage and Static-Load Damage

From the foregoing discussion it appears that the crack-initiation portion of fatigue life is dominated by two damage mechanisms: dislocation dynamics, followed by void growth and coalescence. The same mechanisms of plastic damage are responsible for the yielding and strain-hardening phenomena observed in ductile materials under monotonic loading. As the material is loaded, the number of mobile dislocations begins to increase and the stress-strain response deviates from the elastic line at the proportional limit. From this point on, the intensity of dislocation activity increases with load, reaching a peak before the 0.2 percent yield stress is achieved. Soon after the yield stress is passed, dislocation density is saturated and dislocation movement reaches steady state. (It is worthy of note that the material acoustic emission shows rate characteristics similar to those of the dislocation density rate. This similarity will be utilized in a subsequent section.) Further plastic strain in the strain-hardening region is due to the growth of voids.

The significance of the parallels between fatigue-damage mechanisms and monotonic plasticity processes can be appreciated if these mechanisms are related to the strainranges in which they operate. Figure 5 is a representative model of the various strain components in monotonic stress-strain behavior

of a typical material. At low stress, before bulk plastic deformation occurs, all the strain is nominally elastic, and the elastic-strain line follows the total-strain line at 45° to the horizontal axis. It begins to deviate from the 45° slope at the proportional limit when dislocation dynamics begins to cause plastic strain. By the time 0.2 percent plastic strain has been induced, the dislocation-caused strain rate has approached a saturated level that may or may not be zero. Dislocation-driven strain contribution decays prior to the 0.2 percent yield point because it is superseded by void-driven deformation. Hardening continues as the plastic strain increases, until the plastic-strain curve in figure 5 reaches a slope of 45° , at which time the elastic-strain curve will become horizontal. However, in most materials, failure occurs before this happens.

Failure due to fully reversed cyclic loading may be considered by studying the typical log strain-log life curve, represented in figure 6 by the Morrow formulation (ref. 2), and similarly by Manson (ref. 9) as the method of Universal Slopes. The total strainrange is the arithmetic sum of the elastic and the plastic strainrange components. The plastic strainrange is dominant in low-cycle fatigue, whereas the elastic strainrange dominates in high-cycle fatigue. A transition point, $2N_T$, is defined when the elastic and plastic strain components are equal. The strain, ϵ_T , corresponding to the transition point is marked in the monotonic response curve of figure 5.

Note that the point at which elastic strain and plastic strain are equal may occur well beyond the 0.2 percent yield point and is out of the range of most aeronautical applications. In the case of fatigue loading as well, practical applications frequently fall considerably to the right of $2N_T$ in figure 6, in the region dominated by elastic deformation. At one decade beyond $2N_T$, the plastic strain constitutes less than 25 percent of the total strain. Nevertheless, it reflects the dislocation dynamics responsible for crack-initiation life, just as the proliferation of dislocations is the cause of initial yielding in the monotonic case. Furthermore, crack-initiation life generally accounts for more than 80 percent of life to failure in the elastic region.

ACOUSTIC EMISSION AND DISLOCATION MOTION

In order to assess incremental damage within a test specimen during monotonic or cyclic deformation, measurement is required of some physical parameter whose rate of accrual reflects the rates at which the damage processes occur. At present, no engineering method is readily available for monitoring void formation and development during a mechanical test.

On the other hand, the use of acoustic emission (AE) measurement techniques has become recognized and accepted (refs. 10 to 12) as a relative measure of the amount of dislocation activity in a material specimen. These techniques are based on the fact that dislocation multiplication and motion create minute sounds that are discernible with sensitive acoustic instrumentation. Thus, as the number of free dislocations begins to multiply and the material starts to yield plastically, the material emits acoustically in proportion to the number of dislocations in motion at a given instant.

Figure 7 shows the monotonic response of a typical ductile material (ref. 10). Dislocation motion begins near the material proportional limit and

goes through a maximum at a strain near the middle of the knee of the stress-strain curve. The integral of this rate defines the total free dislocation density count, a curve whose shape reflects the dislocation-driven strain curve in figure 5. The curves representing rate of acoustic emission and total AE count in figure 7 are proportional to free dislocation density rate and total count curves, respectively. Clearly, a definitive relationship for monotonic loading can be formulated between the plastic strain occurring in the knee of the stress-strain curve as a result of dislocation motion and the acoustic emission of the material during yielding.

The stress and strain history and the corresponding rate of acoustic emission during the early cycles of a low-cycle fatigue test on 99.5 percent pure polycrystalline aluminum under symmetric strain cycling (ref. 13) are shown in figure 8. The strain amplitude of ± 0.05 was high and resulted in the material's yielding during both tension and compression. After the massive acoustic emission during initial loading, there was an additional acoustic occurrence during each subsequent yielding in either direction. The emission peaks were approximately equal during subsequent yielding and dropped to the background level (near zero output) during elastic loading and unloading. The almost symmetrical response indicates the facility with which the direction of dislocation motion is reversed under the cyclic shear conditions set up. This is typical of many metals and fully soluble alloys.

What would be the expected acoustic emission response under lower and unsymmetric load conditions? The acoustic emission during the initial cycle of the symmetric loading in figure 8 (shown schematically in fig. 9(a)) is high because of bulk yielding in the material. Under lower symmetrical strain amplitudes, one would expect lower AE peaks corresponding to incipient yielding. Positive mean strain (e.g., $R_\sigma = 0$, as shown schematically in fig. 9(b)), although leading to some asymmetry in stress extrema, causes yielding at both tension and compression reversals at large strain ranges. Thus, the acoustic emission in this case would be expected to be similar to that obtained from symmetrical straining.

At low amplitudes (fig. 9(c)) compressive yielding may not occur, and acoustic emission would be recorded only during tensile loading. Because dislocation motion in this case would be largely unidirectional, the lifetime to saturation, and subsequently to fracture, would be reduced. This effect will probably be even more evident under unsymmetrical stress-cycling conditions. When the stress ratio R_σ is significantly greater than -1 , no compressive yielding occurs and the phenomenon of cyclic strain ratchetting may be observed. Again, if dislocation saturation does not occur as the result of extensive yielding during the initial cycle, further acoustic emission should be recorded during loading in subsequent cycles until saturation is reached. Such a case is shown for carbon-manganese steel (ref. 14) in figure 10, where tensile load reversals produced further acoustic emission until a fatigue crack initiated at a notch. (Because of local compressive yielding at the notch, some AE was noted at times at the minimum load as well. However, it appeared that before crack initiation, the acoustic emission was essentially the result of tensile, rather than compressive, yielding.)

In general it may be conjectured that for metal alloys the dislocation-related fatigue damage which leads to fatigue crack initiation is a function of the maximum strain and stress reached relative to an appropriate yield

criterion. The fatigue-damage rate depends on the rate of dislocation saturation, which, in turn, is a function of a cyclic parameter such as amplitude. This proposal requires further substantiation. In this regard it is of interest that the Goodman diagram in its original form (fig. 1) defined maximum applied stress at the endurance limit as a function of minimum stress as the only cyclic parameter. From the foregoing discussion it appears that the peak stress is a primary parameter affecting the degree of physical damage in a material, and its significance is at least equal to that of the mean stress.

MEAN-STRESS LIFE PARAMETERS

The crux of the preceding discussion is that fatigue damage consists of the gradual exhaustion of dislocation-induced ductile yielding. Such yielding can occur rapidly, either during initial loading or more gradually at the tensile peak of discrete cycles. Morrow (ref. 2) has related the exhaustion concept to the elastic term of the Manson-Coffin relationship in order to predict the effect of mean stress on fatigue life. In terms of stress, his modification takes the form

$$\sigma_a = (\sigma'_f - \sigma_m)(2N_f)^b \quad (1)$$

where σ_a , σ'_f , and σ_m are stress amplitude, a fatigue-related material strength constant, and the mean stress, respectively; $2N_f$ is the number of reversals to crack initiation; and b , a material constant, represents the slope of the basic isothermal (log-log) fatigue curve. For any given lifetime N_f , equation (1) defines a proportional relationship between stress amplitude and mean stress that is dependent on the fatigue-related strength parameter, as in figure 11, a figure immediately recognized as a modified Goodman diagram. As σ_m approaches σ'_f , the amplitude σ_a goes to zero.

Although logic dictates that this relationship is reasonable, the fact is that for most materials the apex of the Goodman diagram along the mean-stress axis does not usually lie at either σ'_f or even σ_{UTS} . Table I presents a comparison of the fatigue-related strength parameter σ'_f and a mean-stress-related strength constant σ'_m , representing the actual apex on the σ_m -axis, for 40 metal alloys. Data for these materials were taken from modified Goodman diagrams appearing in references 15 and 16. Note that for temperatures above approximately 0.4 of the melting temperature (i.e., in the region in which intracrystalline dislocation dynamics are supplanted by grain-boundary sliding as the primary deformation mode), the strength parameters in table I become dependent on frequency as well as on cycle count.

There is no clear correlation between the mean-stress constant σ'_m and either σ'_f or the monotonic strength σ_{UTS} . A typical modified Goodman diagram is shown in figure 12, in this case for 2014-T6, for which $\sigma'_f = 123$ ksi. When the maximum applied stress (the sum of amplitude and mean stress) is elastic and below the proportional limit, the constant-life curves are indeed linear and tend toward a common point ($\sigma'_m = 89$ ksi) on the mean-stress axis. However, when the maximum stress is in the plastic regime, the

curves bend downward and follow the maximum-stress line to the mean-stress axis at the σ_{UTS} intercept. The plastic response reflects the relative insensitivity of low-cycle fatigue to high mean stress discussed previously.

That σ'_f and σ'_m are unrelated should not be surprising. To begin with, although the constants can be looked upon as failure stress in the first cycle and under static loading, respectively, they are in reality no more than graphic intercepts without physical significance. The point σ'_f defines the σ_a -intercept on the $\sigma_a - 2N_f$ plot when $\sigma_m = 0$, and σ'_m defines the σ_m -intercept on the Goodman diagram when $\sigma_a = 0$. Without physical significance, there is no reason for them to be equal. These two disparate concepts are more clearly seen in the three-dimensional Goodman diagram (fig. 13). The position of σ'_f as the point from which the amplitude-lifetime distribution subtends when $R = -1$ is seen on the $\sigma_{max} - \sigma_a$ plane. On the $\sigma_{max} - \sigma_m$ plane, σ'_m is seen to be the focus of the Goodman curves. The familiar Goodman curve family is the projection of the three-dimensional curves in the base plane of the figure.

These considerations lead to the suggestion that the Morrow formulation of equation (1) requires the incorporation of the additional material constant σ'_m in order to anchor the Goodman diagram along the mean-stress axis. The elastic life term then becomes

$$\sigma_a = \sigma'_f \left(1 - \frac{\sigma_m}{\sigma'_m} \right) (2N_f)^b \quad (2)$$

In terms of strain, equation (2) takes the form

$$\Delta \epsilon_{e1} = \frac{2\sigma'_f}{E} \left(1 - \frac{\sigma_m}{\sigma'_m} \right) (2N_f)^b \quad (3)$$

where $\Delta \epsilon_{e1}$ is the elastic strainrange and E is Young's modulus for the material.

The plastic strainrange $\Delta \epsilon_p$, which corresponds to $\Delta \epsilon_{e1}$ as given by equation (3), must take the form

$$\Delta \epsilon_p = 2\epsilon'_f \left(1 - \frac{\epsilon_{mp}}{\epsilon'_{mp}} \right) (2N_f)^c \quad (4)$$

In equation (4), ϵ_{mp} is the plastic strain increment corresponding to σ_m in any given cycle, and ϵ'_f and ϵ'_{mp} represent ductility terms corresponding to the strength constants σ'_f and σ'_m , respectively; c is the universal-slopes constant, usually close to 0.6 in value. A combination of equations (3) and (4) gives the total strain amplitude for a given number of cycles N_f as

$$\frac{\Delta \epsilon}{2} = \frac{\sigma_f'}{E} \left(1 - \frac{\sigma_m}{\sigma_m'}\right) (2N_f)^b + \epsilon_f' \left(1 - \frac{\epsilon_{mp}}{\epsilon_{mp}'}\right) (2N_f)^c \quad (5)$$

An analysis of the mean-stress modified strain-life equation (eq. (5)) shows that it is sensitive to the recorded effect of tensile mean stress. In the plasticity term on the right side of the equation, ϵ_{mp}' is on the order of ϵ_f' . The value of mean plastic strain ϵ_{mp} is set during the initial loading in the first cycle, and decreases thereafter as a result of mean stress wash-out. Thus, the ratio $\epsilon_{mp}/\epsilon_{mp}'$ is seldom greater than 0.05 for ductile materials. Therefore, even in low-cycle fatigue (LCF) when the plastic-strain term dominates fatigue life prediction, the mean strain has negligible effect on life and can safely be ignored.

The mean-stress term also has negligible effect on predicted fatigue life in low-cycle fatigue. Under LCF conditions, the mean-stress ratio σ_m/σ_m' can be large. In this region, however, the elastic strain is in any case small compared with the dominant plastic strain, so that the mean stress is not felt in the total strain. Although σ_m/σ_m' must decrease as fatigue life increases, in high-cycle fatigue the elastic-strain term dominates equation (5), so that the amount of mean stress effectively modifies the total strain at any given life.

From the foregoing it is clear that equation (5) may be simplified for design purposes to

$$\frac{\Delta \epsilon}{2} = \frac{\sigma_f'}{E} \left(1 - \frac{\sigma_m}{\sigma_m'}\right) (2N_f)^b + \epsilon_f' (2N_f)^c \quad (6)$$

Maximum gross stress σ_{max} can never be larger than the material strength σ_{UTS} . Therefore, σ_m' should be replaced by a term related to σ_{UTS} in equation (6) when the maximum stress (given by $\sigma_a + \sigma_m$) exceeds the stress σ_{dp} at which dislocation motion reaches its peak in the material. Under such circumstances, equation (6) becomes

$$\frac{\Delta \epsilon}{2} = \frac{\sigma_f'}{E} \left(1 - \frac{\sigma_m}{Y}\right) (2N_f)^b + \epsilon_f' (2N_f)^c \quad (7)$$

for

$$(\sigma_a + \sigma_m) > \sigma_{dp}$$

where

$$Y = \frac{\sigma_f' \sigma_{UTS} (\sigma_m' - \sigma_{dp})}{\sigma_f' (\sigma_m' - \sigma_{UTS}) + \sigma_m' (\sigma_{UTS} - \sigma_{dp})} \quad (8)$$

For most materials, values for σ_{dp} are not yet tabulated. However, a reasonable approximation is obtained by assuming that the dislocation peak occurs at or near the 0.1 percent offset stress σ_{001} ; that is,

$$\sigma_{dp} \approx \sigma_{001} \quad (9)$$

In table I, σ_{001} values have been tabulated for 40 materials for use in equations (7) and (8).

BITHERMAL FATIGUE

Most engineering applications involving elevated temperatures are subject to thermomechanical cycling; that is, thermal and mechanical cyclic loading occur simultaneously. The complexities of thermomechanical analysis can in large part be circumvented while still retaining the important characteristics of thermomechanical fatigue (TMF) conditions by use of a testing procedure known as bithermal fatigue (ref. 17). In bithermal fatigue, tensile and compressive halves of the loading cycle are imposed isothermally at two extreme temperatures. Temperature changes are permitted to occur only under constant-load (preferably zero-load) conditions. In this way, mechanical strains and strains due to thermal expansion are easily separated in the analysis of data. The higher temperature in the bithermal fatigue cycle is usually in the thermally activated region where oxidation and creep can occur, while the lower temperature is in the region where such time-dependent response is minimal. Thus, the mechanisms of cyclic damage are easier to interpret for discrete bithermal cycles than for the continuously varying TMF cycle just so long as the microstructural changes in the temperature region are comparable.

Under elastic bithermal cycling, a modified Goodman curve may be derived from equation (2). If subscript 1 refers to the temperature at which tension is applied and subscript 2 refers to the temperature at which compressive loading is applied, then at any given lifetime N_{fm}

$$\frac{1}{(2N_{fm})^b} = \frac{\frac{\sigma'_{f1}}{E_1^2} (\sigma'_{m1} - \sigma_{max}) + \frac{\sigma'_{f2}}{E_2^2} (\sigma'_{m2} - \sigma_{min})}{\frac{\sigma'_{m1} \sigma_{max}}{E_1^2} - \frac{\sigma'_{m2} \sigma_{min}}{E_2^2}} \quad (10)$$

If σ'_f/E and σ'_m/E are constants independent of temperature, then σ'_f/σ'_m is also independent of temperature, and equation (10) reduces to the relation

$$\frac{1}{(2N_{fm})^b} = \frac{1}{(2N_{f0})^b} - v_{e1} \left(\frac{\sigma'_f}{\sigma'_m} \right) \quad (11)$$

in which

$$V_{e1} = \frac{1 + R_{\sigma} \left(\frac{E_1}{E_2} \right)}{1 - R_{\sigma} \left(\frac{E_1}{E_2} \right)} \quad (12)$$

and N_{f0} is the lifetime under zero mean stress (cf. ref. 14).

CONCLUSIONS

Fatigue damage in the crack-initiation region is the result of dislocation multiplication and motion, followed after dislocation saturation by void growth and coalescence. Void growth is largely unaffected by the presence of mean stress, but the rate of achieving dislocation saturation is dependent upon both mean and maximum stresses. The rate of dislocation saturation is reflected in material acoustic emission. It is proposed that a series of high-cycle fatigue tests (including mean stress), using acoustic emission techniques in addition to conventional transducers, will lead to an understanding of mean-stress effects under isothermal and bithermal conditions. On the basis of preliminary acoustic emission data and published mean-stress life data, a tentative modification of the Morrow formulation was put forward for fatigue life in the presence of mean stress. This modification depends on a parameter related to the mean stress, and the monotonic stress at which the dislocations in the material reach saturation. The latter stress is approximately the 0.1 percent offset yield stress.

REFERENCES

1. Halford, G.R.; and Nachtigall, A.J.: Strainrange Partitioning Behavior of an Advanced Gas Turbine Disk Alloy AF2-1DA. *J. Aircraft*, vol. 17, no. 8, Aug. 1980, pp. 598-604.
2. Morrow, J.: Fatigue Properties of Metals. *Fatigue Design Handbook*, J.A. Graham, J.F. Millan, and F.J. Appl, eds., SAE, 1968, pp. 21-29.
3. Goodman, J.: *Mechanics Applied to Engineering*, 9th Edition. Longmans, Green, and Co., London, 1899, p. 634.
4. Landgraf, R.W.: The Resistance of Metals to Cyclic Deformation. *High Fatigue Resistance in Metals and Alloys*, ASTM-STP-467, ASTM, Philadelphia, PA, 1970, pp. 3-36.
5. Laird, C.: *Mechanisms and Theories of Fatigue*. Fatigue and Microstructure, ASM, Metals Park, OH, 1978, pp. 149-203.
6. Lin, T.H.: Micromechanics of Fatigue Crack Initiation - Theory and Experimental Observations. *Mechanics of Fatigue*, T. Mura, ed., ASME, 1981, pp. 91-109.
7. Grobstein, T.L.: *Fatigue Damage to Nickel Prior to Crack Initiation*. Case Western Reserve University, 1986.

8. Wilsdorf, H.G.F.: Direct Studies of Fracture Mechanisms in Metals at Highest Magnification. Dept. of Materials Science, University of Virginia, Report No. UVA/525354/MS82/102, 1982. (Avail. NTIS, AD-A114712.)
9. Manson, S.S.: Fatigue: A Complex Subject - Some Simple Approximations. Exp. Mech., vol. 5, no. 7, July 1965, pp. 193-226.
10. Heiple, C.R.; and Carpenter, S.H.: Acoustic Emission from Dislocation Motion. Acoustic Emission, J.R. Matthews, ed., Gordon and Breach, New York, 1983, pp. 15-103.
11. Buck, O.; and Alers, G.A.: New Techniques for Detection and Monitoring of Fatigue Damage. Fatigue and Microstructure, ASM, Metals Park, OH, 1978, pp. 101-147.
12. Heiple, C.R.; Carpenter, S.H.; and Thomas, R.L.: Acoustic Emission Produced by Deformation of Metals and Alloys. Rockwell International Corp., Report No. RFP-4046, Golden, CO, Mar. 1987.
13. Kishi, T., et al.: The Application of Acoustic Emission Technique to the Study of Strain Hardening and Fatigue Hardening. Third Acoustic Emission Symposium, Japan Industrial Planning Assoc., Tokyo, 1976, pp. 305-325.
14. Palmer, I.G.: Acoustic Emission Measurements on Reactor Pressure Vessel Steel. Mater. Sci. Eng., vol. 11, 1973, pp. 227-236.
15. Metallic Materials and Elements for Aerospace Vehicle Structures. DOD MIL-HDBK-5C, 1979.
16. Aerospace Structural Metals Handbook. Metals and Ceramics Information Center, Battelle Labs, Columbus, OH, 1988.
17. Halford, G.R.: Low-Cycle Thermal Fatigue. Thermal Stresses II, R.B. Hetnarski, ed., Elsevier Press, 1987, pp. 330-428.

TABLE I. - STRENGTH PARAMETERS FOR GOODMAN DIAGRAM
 [Material strength, σ_{UTS} ; one-tenth percent offset stress, σ_{001} ; fatigue-related strength, σ_f ; mean-stress-related strength, σ_m .]

Material	Monotonic		Cyclic	
	σ_{UTS}	σ_{001}	σ'_f	σ'_m
Stress, σ , ksi				
Steels				
PH15-7Mo (TH1050)	200	186	429	251
PH15-7Mo (TH1050), 500 °F	178	140	250	224
17-4PH (H900)	201	177	513	335
17-4PH (H1025)	165	162	205	275
Custom 450 (H900)	192	174	551	340
Custom 450 (H1050)	155	143	392	213
PH13-8Mo (H1000)	217	201	440	360
AISI 4340 (150 ksi)	159	147	209	339
AISI 4340 (200 ksi)	208	187	510	263
15-5PH (H1025), L	164	162	340	380
15-5PH (H1025), LT	164	150	340	223
Custom 455 (H1000)	213	198	280	280
Aluminum alloys				
2014-T6	73	61	123	89
2024-T3	73	51	155	106
2024-T4	77	52	155	154
2219-T851	66	48	170	72
6061-T6	44	40	125	85
7075-T6 (sheet)	82	70	192	90
7075-T6 (wrought)	87	72	168	113
Titanium alloys				
6Al-4V Plate (75 °F)	154	144	260	188
6Al-4V Sheet (75 °F)	172	146	300	240
6Al-4V Sheet (600 °F)	132	100	205	243
6Al-4V Sheet (800 °F) ^a	124	88	180	246
13V-11Cr-3Al (75 °F)	138	128	125	284
13V-11Cr-3Al (600 °F)	116	98	135	(b)
13V-11Cr-3Al (800 °F)	116	94	110	(b)
Nickel alloys				
Inconel 718 (75 °F)	198	198	285	198
Inconel 718 (1000 °F)	c ₁₇₉	140	100	1.7 σ_{UTS}
	d ₁₆₅	140	100	1.7 σ_{UTS}
	e ₁₅₄	140	100	1.7 σ_{UTS}
Inconel 718 (1200 °F)	c ₁₃₀	125	68	4.39 σ_{UTS}
	d ₁₁₀	125	68	4.39 σ_{UTS}
	e ₉₀	125	68	4.39 σ_{UTS}
Waspaloy (1200 °F) ^a	160	100	370	229
Nimonic 90 (1100 °F)	100	100	100	180
MAR-M247 (75 °F)	140	100	325	187
MAR-M247 (1600 °F)	120	85	395	187
Inconel 751 (1350 °F)	d ₇₂	66	168	168
	e ₅₉	66	168	168
Inconel 751 (1500 °F)	d ₃₈	---	270	63
	e ₂₂	---	270	63
Udimet 500 (1200 °F)	d ₁₂₀	70	123	226
	e ₁₀₈	70	123	226
Udimet 500 (1650 °F)	c ₅₀	50	195	1.4 σ_{UTS}
	d ₃₂	50	195	1.4 σ_{UTS}
	e ₂₀	50	195	1.4 σ_{UTS}
Cobalt alloys				
S-816	150	66	88	175
Cast X-40 (1200 °F)	c ₉₃	57	57	1.5 σ_{UTS}
	d ₈₂	57	57	1.5 σ_{UTS}
	e ₇₀	57	57	1.5 σ_{UTS}

^aRate dependent.

^bGoodman diagram concave up at $R < 0$.

^c1 hr, 2.16×10^5 cycles.

^d10 hr, 2.16×10^6 cycles.

^e100 hr, 2.16×10^7 cycles.

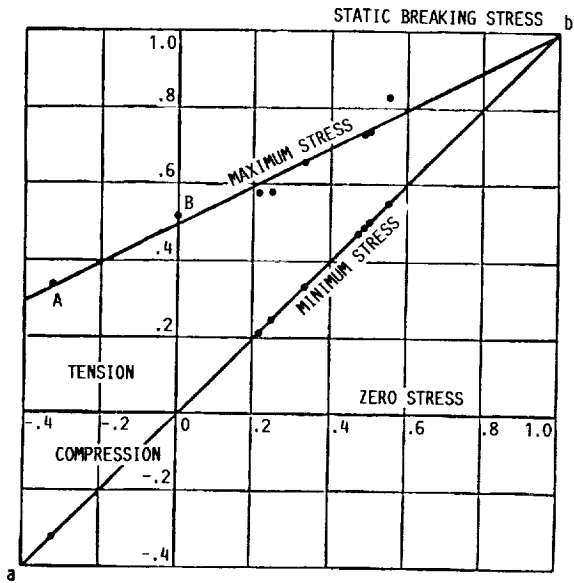


FIGURE 1. - GOODMAN DIAGRAM.

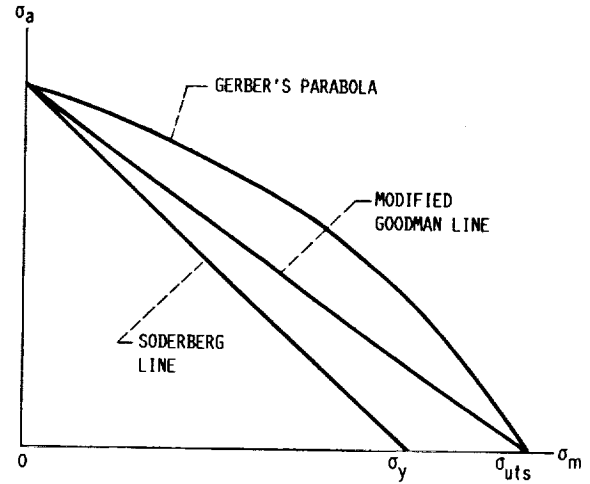


FIGURE 2. - MODIFIED GOODMAN DIAGRAM.

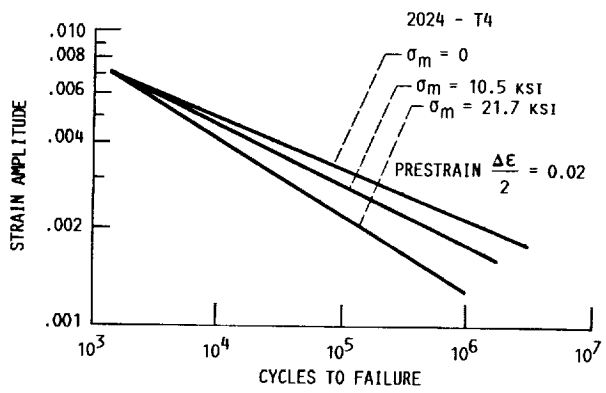


FIGURE 3. - FATIGUE LIFETIMES WITH MEAN STRESSES.

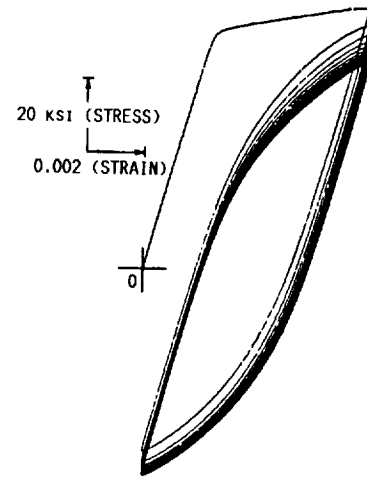


FIGURE 4. - RELAXATION OF MEAN STRESS IN SAE 1045 STEEL (REF. 8).

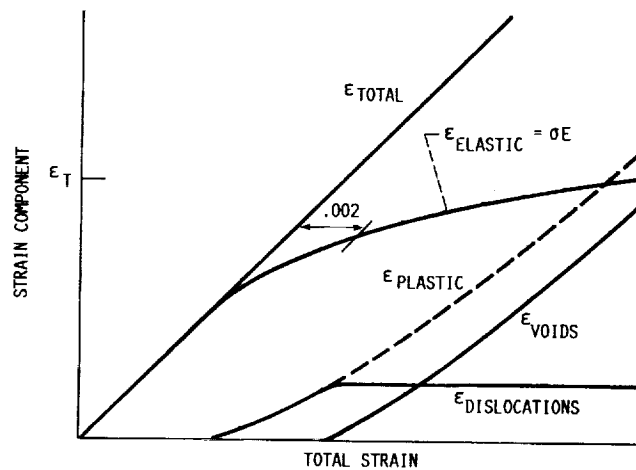


FIGURE 5. - STRAIN COMPONENTS OF ELASTOPLASTIC RESPONSE DURING TENSILE TEST.

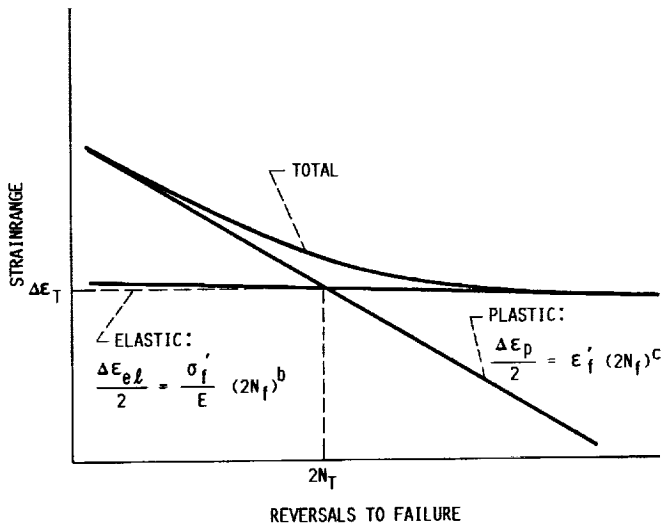


FIGURE 6. - FATIGUE LIFE RELATION (REF. 2).

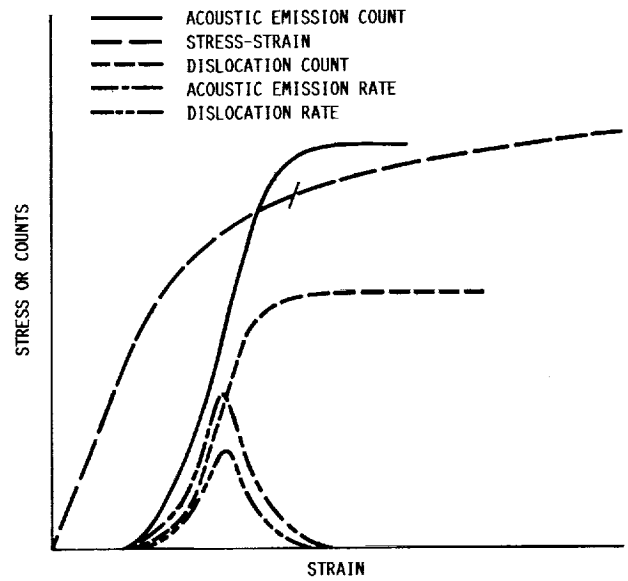


FIGURE 7. - ACOUSTIC EMISSION RESPONSE UNDER MONOTONIC LOADING.

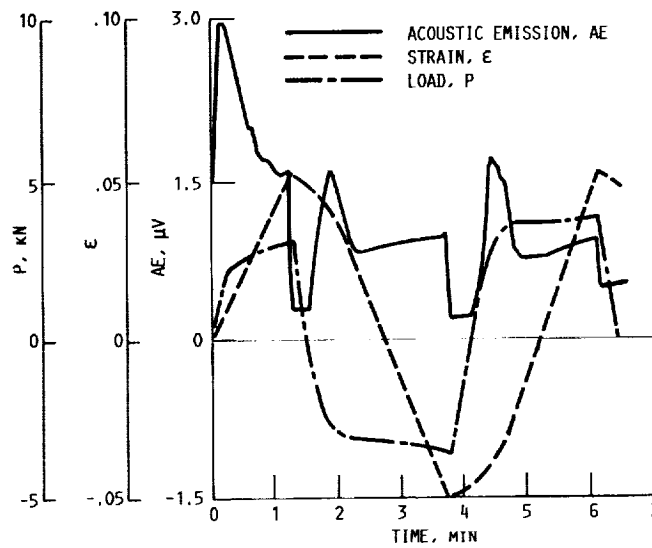


FIGURE 8. - ACOUSTIC EMISSION DURING CYCLIC LOADING OF ALUMINUM (REF. 13).

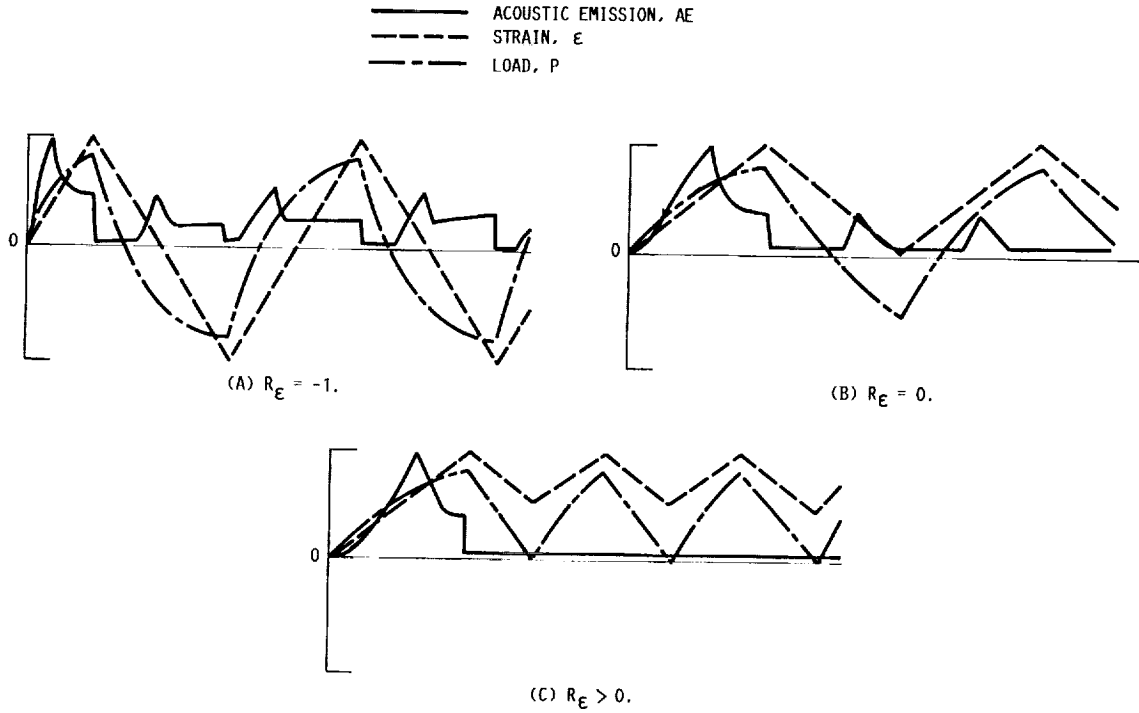


FIGURE 9. - SCHEMATIC OF POSSIBLE ACOUSTIC EMISSION RESPONSE WITH MEAN STRESS.

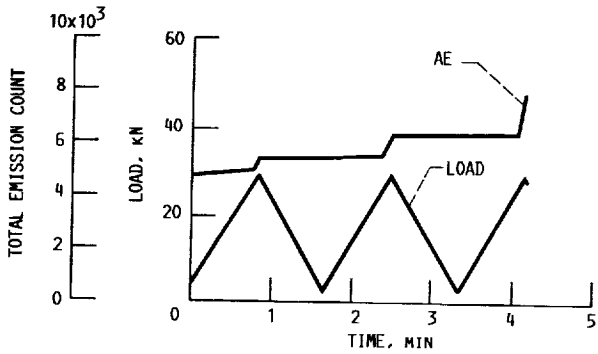


FIGURE 10. - ACOUSTIC EMISSION DURING CYCLIC LOADING OF C-Mn STEEL (REF. 14).

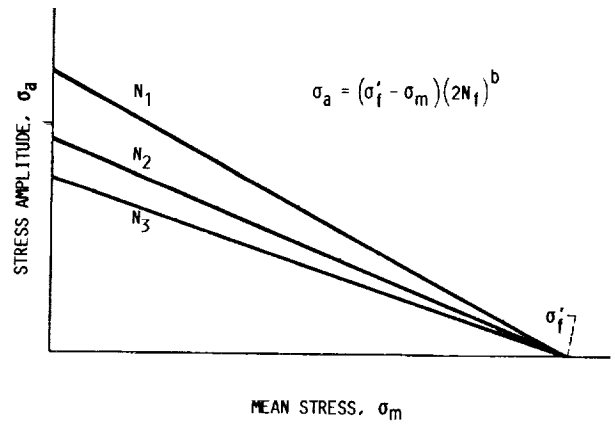


FIGURE 11. - MORROW MEAN-STRESS LIFE FORMULATION (REF. 2).

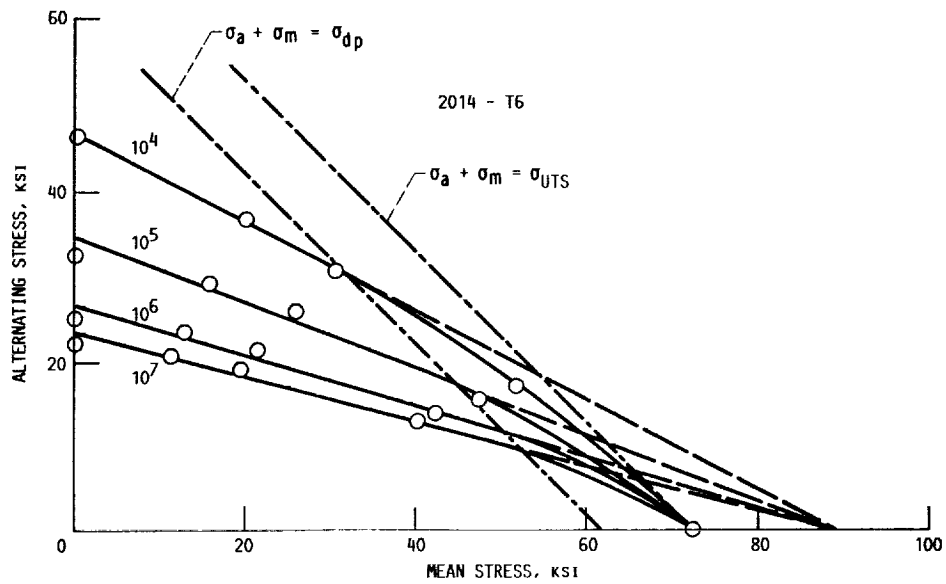


FIGURE 12. - REINTERPRETATION OF MODIFIED GOODMAN DIAGRAM.

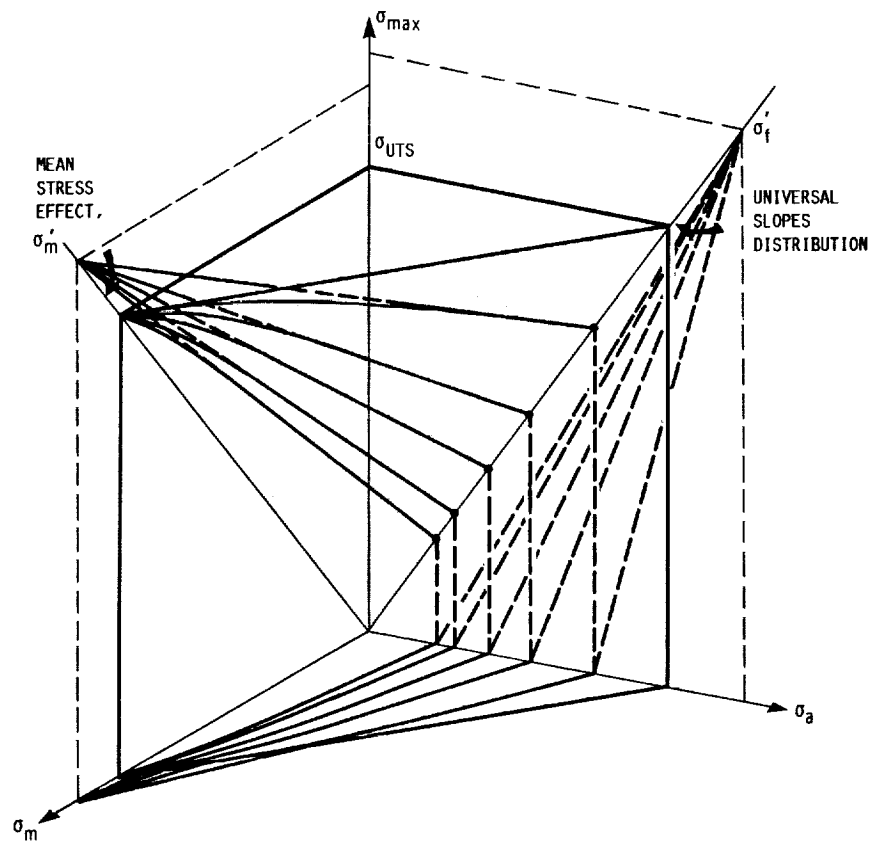


FIGURE 13. - THREE-DIMENSIONAL MODIFIED GOODMAN DIAGRAM.

1. Report No. NASA TM-101311		2. Government Accession No.		3. Recipient's Catalog No.	
4. Title and Subtitle Mean Stress and the Exhaustion of Fatigue-Damage Resistance				5. Report Date November 1989	
				6. Performing Organization Code	
7. Author(s) Avraham Berkovits				8. Performing Organization Report No. E-4307	
				10. Work Unit No. 582-01-11	
9. Performing Organization Name and Address National Aeronautics and Space Administration Lewis Research Center Cleveland, Ohio 44135-3191				11. Contract or Grant No.	
				13. Type of Report and Period Covered Technical Memorandum	
12. Sponsoring Agency Name and Address National Aeronautics and Space Administration Washington, D.C. 20546-0001				14. Sponsoring Agency Code	
15. Supplementary Notes Avraham Berkovits, National Research Council—NASA Research Associate, on leave from Technion—Israel Institute of Technology, Haifa, Israel.					
16. Abstract <p>Mean-stress effects on fatigue life are critical in isothermal and thermomechanically loaded materials and composites. Unfortunately, existing mean-stress life-prediction methods do not incorporate physical fatigue-damage mechanisms. An objective of this paper is to examine the relation between mean-stress-induced damage (as measured by acoustic emission) and existing life-prediction methods. Acoustic emission instrumentation has indicated that, as with static yielding, fatigue damage results from dislocation buildup and motion until dislocation saturation is reached, after which void formation and coalescence predominate. Correlation of damage processes with similar mechanisms under monotonic loading led to a reinterpretation of Goodman diagrams for 40 alloys and a modification of Morrow's formulation for life prediction under mean stresses. Further testing, using acoustic emission to monitor dislocation dynamics, can generate data for developing a more general model for fatigue under mean stress.</p>					
17. Key Words (Suggested by Author(s)) Metal fatigue; Life prediction; Mean stress; Strain fatigue; Endurance limit; Thermomechanical fatigue; Acoustic emission; Dislocations; Void growth			18. Distribution Statement Unclassified—Unlimited Subject Category 39		
19. Security Classif. (of this report) Unclassified		20. Security Classif. (of this page) Unclassified		21. No of pages 17	22. Price* A03

